Snow dunes: A controlling factor of melt pond distribution on Arctic sea ice

Chris Petrich,[1,2] Hajo Eicken,[1,3] Christopher M. Polashenski,[4] Matthew Sturm,[4] Jeremy P. Harbeck,[1,5] Donald K. Perovich,[6] and David C. Finnegan[6]

Received 7 May 2012; revised 31 July 2012; accepted 21 August 2012; published 25 September 2012.

[1] The location of snow dunes over the course of the ice-growth season 2007/08 was mapped on level landfast first-year sea ice near Barrow, Alaska. Landfast ice formed in mid-December and exhibited essentially homogeneous snow depths of 4–6 cm in mid-January; by early February distinct snow dunes were observed. Despite additional snowfall and wind redistribution throughout the season, the location of the dunes was fixed by March, and these locations were highly correlated with the distribution of meltwater ponds at the beginning of June. Our observations, including ground-based light detection and ranging system (lidar) measurements, show that melt ponds initially form in the interstices between snow dunes, and that the outline of the melt ponds is controlled by snow depth contours. The resulting preferential surface ablation of ponded ice creates the surface topography that later determines the melt pond evolution.

Citation: Petrich, C., H. Eicken, C. M. Polashenski, M. Sturm, J. P. Harbeck, D. K. Perovich, and D. C. Finnegan (2012), Snow dunes: A controlling factor of melt pond distribution on Arctic sea ice, *J. Geophys. Res.*, *117*, C09029, doi:10.1029/2012JC008192.

1. Introduction

[2] The Arctic sea-ice cover is sensitive to the solar heat input particularly in late spring and early summer [*Perovich et al.*, 2007]. At this time, the mean ice surface albedo decreases significantly due to the onset of melt, the loss of snow, and the formation of melt ponds [*Perovich*, 1998; *Hanesiak et al.*, 2001; *Grenfell and Perovich*, 2004; *Perovich and Polashenski*, 2012]. Melt ponds have a low albedo, absorb greater amounts of energy, and are the location of preferential ice melt [*Eicken et al.*, 2002; *Lüthje et al.*, 2006], thereby contributing to the structural disintegration and decay of melting ice [e.g., *Light et al.*, 2008; *Petrich et al.*, 2012]. They are also preferential pathways of light transmission potentially increasing biological productivity significantly [*Arrigo et al.*, 2012]. Pond formation and evolution on multiyear sea ice has been found to be dominated by surface topography shaped during previous melt seasons [e.g., *Morassutti and LeDrew*, 1996; *Eicken et al.*, 2004]. However, on first-year sea ice, field observations and modeling have shown that the overall snow depth on the ice may impact pond formation, mostly through superimposed ice formation and by covering surface meltwater [*Eicken et al.*, 2004; *Lüthje et al.*, 2006]. Furthermore, it has been shown that the early stages of pond formation determine pond evolution through the melt season [*Holt and Digby*, 1985; *Eicken et al.*, 2002; *Polashenski et al.*, 2012].

[3] Since snow typically exhibits spatial variability at short length scales (10 to 20 m) on sea ice [*Barnes et al.*, 1979; *Sturm et al.*, 2002; *Iacozza and Barber*, 2010], these earlier findings raise the question as to how such depth variations affect pond development. Snow depth distribution patterns are related to the degree of deformation of the underlying ice surface [*Fetterer and Untersteiner*, 1998; *Herzfeld et al.*, 2006] and the interaction between drifting snow particles and the underlying ice surface in relation to the wind speed [*Massom et al.*, 2001]. However, little is known about the initiation of snow dune formation on undeformed surfaces [cf. *Iacozza and Barber*, 2010]. In this study, we examined linkages between snow depth distribution and pond formation on level first-year sea ice and investigated how early stage melt pond patterns related to the snow topography established months earlier. This work links observations of the snow cover on sea ice [e.g., *Barnes et al.*, 1979] with the later stages of melt pond evolution after ponds have started form [*Polashenski et al.*, 2012]. It highlights the fundamental importance of the winter snow regime on the summer decay

[1]Geophysical Institute, University of Alaska Fairbanks, Fairbanks, Alaska, USA.
[2]Northern Research Institute, Narvik, Norway.
[3]International Arctic Research Center, University of Alaska Fairbanks, Fairbanks, Alaska, USA.
[4]U.S. Army Cold Regions Research and Engineering Laboratory–Alaska, Fort Wainwright, Alaska, USA.
[5]NASA Goddard Space Flight Center, Greenbelt, Maryland, USA.
[6]U.S. Army Cold Regions Research and Engineering Laboratory, Hanover, New Hampshire, USA.

Corresponding author: C. Petrich, Northern Research Institute, P.O. Box 250, NO-8504 Narvik, Norway. (christian.petrich@norut.no)

0148-0227/12/2012JC008192

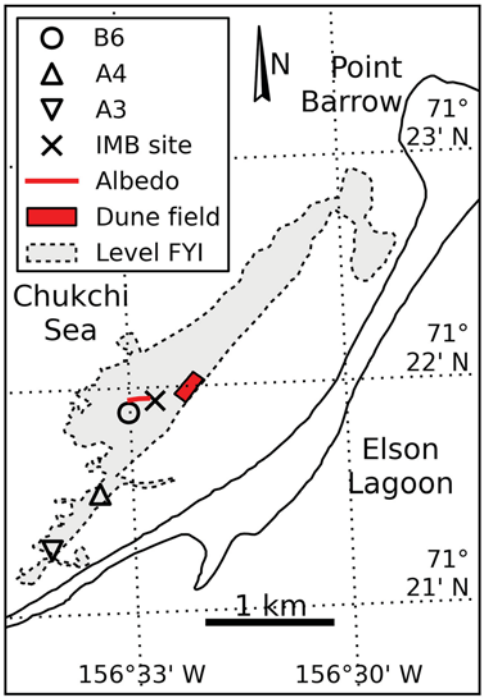

Figure 1. Map of the study site on landfast sea ice in the Chukchi Sea near Point Barrow, Alaska.

of sea ice and also sheds light on the formation of spatial patterns characteristic of ponds on level sea ice.

2. Methods

[4] Snow on sea ice forms characteristic patterns, barchans in the presence of ample snow and wind, and erosional sastrugi features [*Doumani*, 1967; *Watanabe*, 1978; *Sturm*, 2009]. We refer to all these features collectively as dunes for simplicity. While ideally the relationship between snow dunes in winter and melt pond patterns in summer would have been established using repeat surveys by aerial photography or a light detection and ranging system (lidar), this was not possible: low temperatures and poor contrast between snow and ice pose challenges for lidar measurements and aerial photography, respectively. Instead a more rugged approach was used. Depth probing and a single lidar survey allowed us to record the snow surface elevation throughout winter and establish a statistical relation between it and the summer surface as revealed by aerial photography.

[5] Two aspects have to be distinguished: the mobility of dunes throughout winter, and the spatial relationship between dunes and melt ponds. Snow dune centers were tracked through the winter in an area 200 m × 100 m that was staked off in February 2008. By this time, the snow dunes were already established and a single GPS (Garmin GPS-16HVS) and snow depth measurement was taken at the highest point near the center of each dune. Position measurements were performed with a Wide Area Augmentation System (WAAS)-enabled GPS receiver. The horizontal accuracy of WAAS-equipped receivers at Barrow has been determined to have been better than 1.2 m 95% of the time between January and June 2008 [*Federal Aviation Administration*, 2008a, 2008b]. This is less than the size of observed dunes, and the impact of this potential error will be discussed. Dunes were recorded on 8 February, and again on 19 March, and 16 April.

[6] The study site was located on undeformed landfast sea ice, approximately 4 km southwest of Point Barrow (Figure 1). It consisted of a stationary ice mass balance probe (IMB), an albedo line, and an area dedicated to snow dune tracking. The stable landfast ice cover there was established on 15 December 2007 when ice drifted toward shore and formed stabilizing pressure ridges seaward of the dune field. Level congelation ice formed in distinct patches shoreward of the ridges, surrounded by deformed ice [*Druckenmiller et al.*, 2009]. The deformed ice South-East of the level ice consisted mainly of consolidated rubble with surface elevation of 0.5 m or less. Smooth ice patches extended for several kilometers parallel and several hundred meters perpendicular to the coast. All measurements discussed here were taken on the patch shown in Figure 1, the outline of which was traced and marked during the ground survey in February.

[7] An IMB probe was installed on the ice on 7 February that recorded ice thickness and temperature, weather data, and snow depth within the 1 m footprint of a downward-looking sonic ranging sensor [*Druckenmiller et al.*, 2009]. Spot measurements of ice thickness were performed with a 5 cm-diameter ice auger at various points across the level ice patch. Additional weather data were obtained from the National Oceanic and Atmospheric Administration (NOAA) for the Barrow airport.

[8] On 7 May, the snow surface elevation of a 25 m × 50 m subsection of the snow dune field was scanned with a Riegl LMS-Z420i ground-based lidar. Data were processed to 0.1 m spatial resolution. Lidar elevation data were recorded relative to the thinnest snow depth in the footprint, which was (3 ± 2) cm deep.

[9] The progression of surface melt was documented with albedo measurements and surface characterizations along a 200 m transect (Figure 1). Measurements were taken in April and, starting 28 May, daily around local noon. The surface conditions along the albedo line were classified as snow, bare ice or white, decaying ice, slushy ice, melt pond, or suspended ice (i.e., a thin new ice sheet above a draining pond). Aerial surveys were conducted on 7 June and 10 June. A Piper aircraft flew at an altitude of 300 m with a downward-looking digital camera (Nikon D40 SLR with 18–55 mm lens, fixed at 24 mm) and timed shutter release. The pixel size was approximately 0.1 m, and the field of view was 200 m along-track by 300 m cross-track.

[10] A composite image was produced with hugin/Panaroma Tools from 3 overlapping aerial photographs from 7 June. The composite was downsampled to 0.2 m resolution with a Lanczos filter for data reduction and georeferenced with an Equidistant Cylindrical Projection [*Snyder*, 1987] and linear transformation accounting for translation, scale, rotation, and shear,

$$\begin{aligned} x &= a_0 + a_1\varphi + a_2\lambda \\ y &= b_0 + b_1\varphi + b_2\lambda, \end{aligned} \tag{1}$$

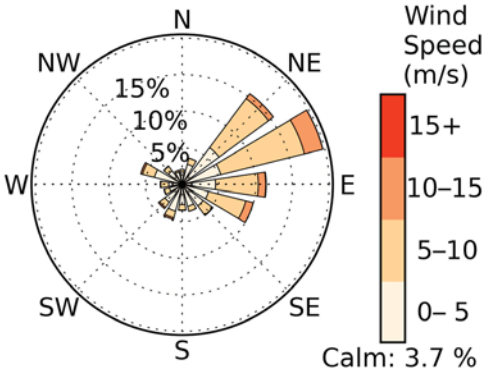

Figure 2. Windrose for sustained winds registered from December 2007 through May 2008, at Barrow, Alaska.

where x and y are pixel coordinates, and φ and λ are latitude and longitude, respectively. The coefficients a_i and b_i were found from least squares minimization of the residual of the coordinates of the four corners of the dune field.

[11] To discriminate ponds from islands of exposed snow or ice, we used the red channel of the aerial composite image because it has the largest contrast between melt pond and snow or ice. The histogram of the red channel of the composite of aerial photographs has two distinct modes when the sea ice surface is partially covered by ponds. The threshold used for discrimination was set as the centerpoint between the two modes (i.e., ponded surface and not ponded surface, respectively).

[12] We tested the observed correspondence of winter dune locations and dry islands in the melt season against the null-hypothesis, i.e., that the observed correlation between dunes and dry islands was due strictly to chance. The probability of observing at least w out of N dunes coinciding with islands of exposed snow or ice by chance is

$$p(N,w,q) = \sum_{k=w}^{N} \binom{N}{k} q^k (1-q)^{N-k}, \tag{2}$$

where q is the probability of coincidence for a single dune, i.e., q is the fractional areal coverage of islands, k is the index of summation, and $\binom{N}{k}$ is a binomial coefficient.

[13] Equation (2) is valid if data are spatially uncorrelated. In order to ensure a conservative estimate of p, we subsampled the ensemble of observations based on correlation lengths of either snow cover or features seen in aerial photographs. Subsampled ensembles were generated enforcing either a minimum distance between any two observations or that no observation falls within an ellipse of specified dimensions around any randomly selected observation. The distances for exclusion were derived from variograms of snow depth transects, and from the correlation function of the aerial photograph, respectively.

[14] Snow depth transects were recorded in the vicinity of the IMB probe with a SnowHydro GPS Magnaprobe [*Sturm and Holmgren*, 1999; *Sturm*, 2009] during campaigns in January through June. The mean (μ) and standard deviation (σ) of each snow transect was calculated, along with the variogram

$$\gamma(h) = \frac{1}{2N_h} \sum_{x_i - x_j = h} \left[z(x_j) - z(x_i) \right]^2, \tag{3}$$

where z is the snow depth at position x_i and x_j, respectively, h is the separation (lag) between x_i and x_j, and N_h is the number of pairs $x_i - x_j = h$. The range, or correlation length, of a variogram is usually defined as the lag h at which the variogram reaches 95% of the limit for $h \to \infty$ [*Sturm et al.*, 2002]. The limit for infinitely long transects with stationary modes (i.e., mean, standard deviation etc.) is σ^2. We determined the range, R_{95}, as the shortest lag at which $\gamma = 0.95\sigma^2$.

[15] The correlation function, ρ, of the red channel was calculated for the level sea ice region of the aerial composite of 7 June. The image size was 640 m × 260 m (640 m in NE–SW direction), and the kernel used for correlation was the center area of 320 m × 130 m. It is

$$\rho(\Delta x, \Delta y) = \frac{1}{\sigma_{img}^2 n} \sum_{\substack{x_{n,k} - x_{n,l} = \Delta x \\ x_{i,m} - x_{j,m} = \Delta y}} \left[\left(r(x_{i,k}) - \mu_{img} \right) - \left(r(x_{j,l}) - \mu_{img} \right) \right]^2, \tag{4}$$

where $-320\ \text{m} \le \Delta x \le 320\ \text{m}$ and $-130\ \text{m} \le \Delta y \le 130\ \text{m}$ are the lag in x and y-direction, respectively, n is the number of pixels in the kernel, r is the value of the red channel, σ_{img}^2 is the variance of the red channel in the kernel, and μ_{img} is the mean value of the red channel of the image.

3. Results

3.1. Snow Cover

[16] Based on weather data of the National Oceanic and Atmospheric Administration (NOAA) for the season 2007/08 at Barrow, the prevailing wind direction was from East to North-East, with typical wind speeds around 5 m/s, reaching 10 m/s and above during episodic storms (Figures 2, 3a, and 3b). Snow drifting (saltation) begins around 5 m/s [*Pomeroy*, 1989], resulting in an almost constant low-level hiss of snow across the surface. However, significant amounts of snow are transported during stronger winds as the flux of wind-blown snow increases with wind speed with a power law function [e.g., *Pomeroy and Gray*, 1995]. For reference, speeds in excess of 7 m/s are highlighted in Figure 3b. Air temperatures stayed below 0°C until the second half of May and approached 0°C during precipitation events in January and on several occasions in April (Figure 3c). Significant precipitation rates were limited to a few discrete events in winter (Figure 3d), although trace precipitation was reported more frequently (not shown). While the quantitative relationship between precipitation reported at the Barrow airport and observed on sea ice is not known, we know from field observations that precipitation fell at approximately the same time (e.g., snow fall occurred around 6 and 28 April, and liquid precipitation around 24 May and 5 June). Figure 3e shows the snow depth history recorded by the IMB probe, and mean and standard deviation of snow depth transects. Snow depth increased significantly after precipitation in late

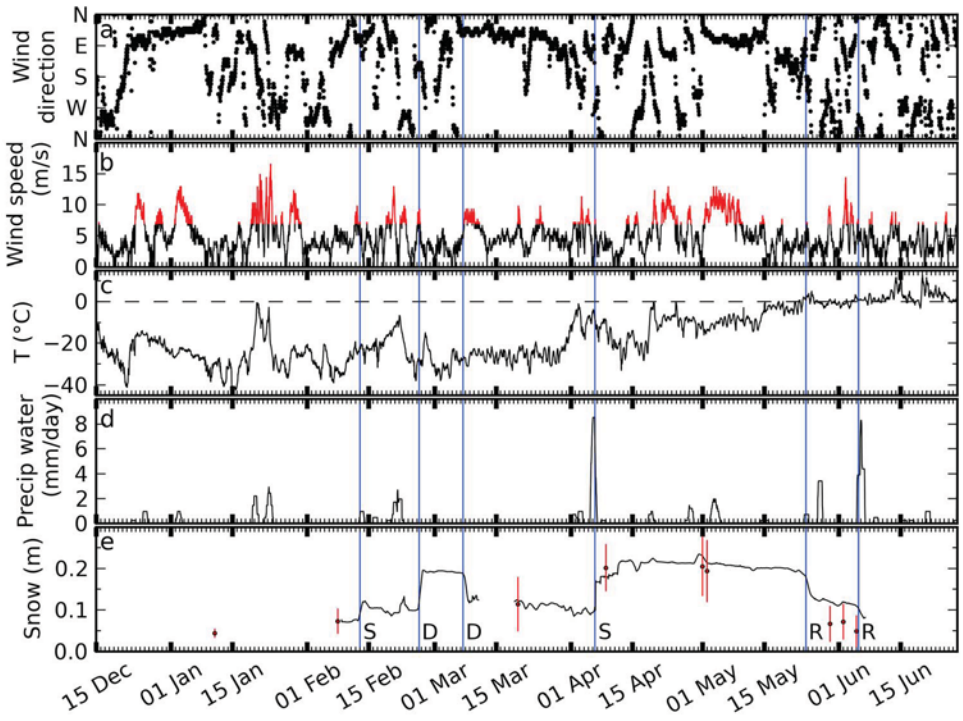

Figure 3. Weather observations reported at the Barrow airport, December 2007 through June 2008: (a) wind direction, (b) wind speed (winds in excess of 7 m/s are shown in red), (c) air temperature, (d) water-equivalent precipitation, and (e) SIZONET snow depth measurements on sea ice of the IMB probe (line) and snow depth transects (dots with vertical bars indicating ± 1 standard deviation around the mean). Time base is UTC. Vertical lines indicate dates of precipitation of snow (S) and rain (R), and of snow drift (D).

January and 12 February. On 26 February and 7 March snow depth recorded at the IMB site changed significantly in response to winds in excess of 7 m/s. The increase in snow depth on 6 April and decrease on 24 May and 5 June coincided with precipitation of snow (April) and liquid (May and June), respectively.

[17] Snow depth transects show that the depth distribution was narrow in January (standard deviation 0.01 m) and increased to reach a maximum in early May (standard deviation 0.08 m, Table 1). 200 m-excerpts of selected transects are shown in Figure 4, revealing an almost completely featureless homogeneous snow cover in January, the presence of distinct, well-separated dunes in February, and a snow cover rich in topographic features from March onward.

[18] The variograms of the snow depth transects are generally consistent, showing γ/σ^2 increased to near 1 within 2 to 15 m (Figure 5), with the range (structural length) falling between 2.5 and 10 m for 67% of the transects (Table 1).

[19] Co-located snow depth and ice thickness measured on 29 April and 1 May show a significant association with the thickest ice recorded under the thinnest snow (Figure 6). The two-sided p-value is $p = 0.0006$ for a hypothesis test whose null hypothesis is that the slope of a linear fit is zero.

3.2. Dune Locations

[20] The number of dunes and dune height increased throughout the season. A total of 47, 122, and 147 dunes were identified and their locations recorded on 8 February, 19 March, and 16 April, respectively. The recorded heights

Table 1. Statistics of Barrow Snow Depth Transects in 2008, With Mean μ, Standard Deviation σ, and Range of the Variogram, R_{95}

Date	Length (m)	Direction (deg)	Step Δx (m)	Mean μ (m)	Std σ (m)	Range R_{95} (m)
10 Jan	244[a]	−48	0.7	0.044	0.0094	7.2
7 Feb	316[a]	−52	1.6	0.073	0.028	8.8
	471	51	1.6	0.073	0.031	6.8
19 Mar	318	−32	0.7	0.12	0.074	10.4
	510[a]	51	0.6	0.11	0.058	16.1
8 Apr	197	118	0.5	0.20	0.057	19.6
	243	−61	0.5	0.21	0.059	8.9
	198[a]	−146	0.4	0.18	0.058	5.3
	134	33	0.4	0.17	0.039	3.7
	204	−62	0.4	0.22	0.058	22.9
	157	119	0.4	0.21	0.050	21.8
	191	33	0.5	0.20	0.048	7.7
	193	−146	0.4	0.21	0.052	8.6
30 Apr	521[a]	−130	0.4	0.21	0.070	7.6
1 May	145	−43	0.7	0.19	0.081	8.3
	104	−16	0.7	0.22	0.070	5.1
	545[a]	−129	0.8	0.19	0.071	9.0
29 May	235[a]	40	1.4	0.066	0.038	5.9
	107	125	1.4	0.063	0.052	6.2
	106	126	1.4	0.063	0.040	2.5
1 Jun	111	−53	1.4	0.069	0.041	5.7
	232[a]	40	1.5	0.070	0.038	5.6
	107	124	1.3	0.066	0.040	7.4
	530	−129	1.5	0.076	0.045	19.2
	196	85	1.2	0.067	0.039	13.7
4 Jun	526[a]	51	1.3	0.047	0.038	28.9
	528	−129	3.0	0.054	0.035	12.9

[a]Transects of Figures 4 and 5.

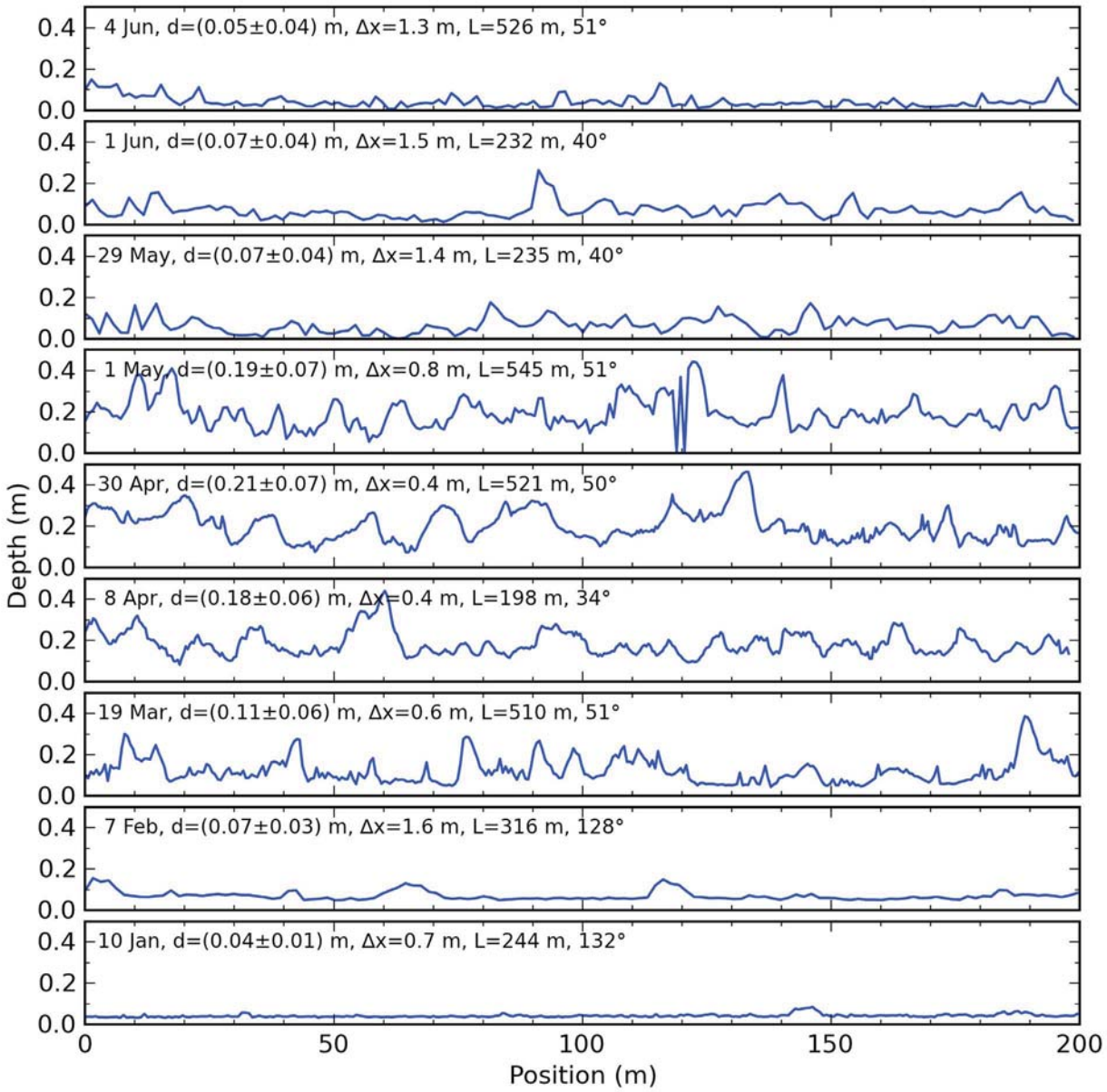

Figure 4. Selected snow depth transects. Each plot indicates date, mean and standard deviation of the transect (d), measurement interval (Δx), transect length (L), and direction in degrees east of North.

(assuming a smooth ice substrate) were 0.16 ± 0.04 m, 0.31 ± 0.07 m, and 0.33 ± 0.06 m, respectively. The areal extent ranged from 130 to 430 m^2 per dune, which is equivalent to dune radii ranging from 6 to 12 m, i.e., the same magnitude as the correlation lengths of transects (Table 1). Figure 7 shows the recorded dune locations superimposed on the aerial composite of 7 June. The recorded locations coincide predominantly with white "islands" between meltwater ponds. Using the red channel in the aerial photo images for discriminating between ponds and unponded snow/ice islands, 49% of all pixels in the dune field classify as islands (i.e., $q = 0.49$, equation (2)). Based on this threshold, 35 (75%), 119 (98%), and 131 (89%) of all dune locations of February, March and April, respectively, were co-located with islands in June (Figure 7).

[21] The correlation function of the composite aerial photograph of 7 June is shown in Figure 8a. The spatial correlation is most pronounced in direction 76° east of North (major axis), i.e., parallel to the dominant direction of the wind, and least pronounced perpendicular to this direction (minor axis). The first zero crossing along the minor axis is at 7.5 m, while the zero crossing along the major axis is at 45 m (Figure 8b). As revealed by the aerial survey, the melt pond pattern in the study area was indistinguishable from the melt pond pattern observed throughout the level ice patch shown in Figure 1. Specifically, there was no evidence the consolidated rubble to the southeast of the field influenced the melt pond pattern.

[22] Lidar measurements of the two-dimensional snow depth distribution of 7 May show that snow depth and

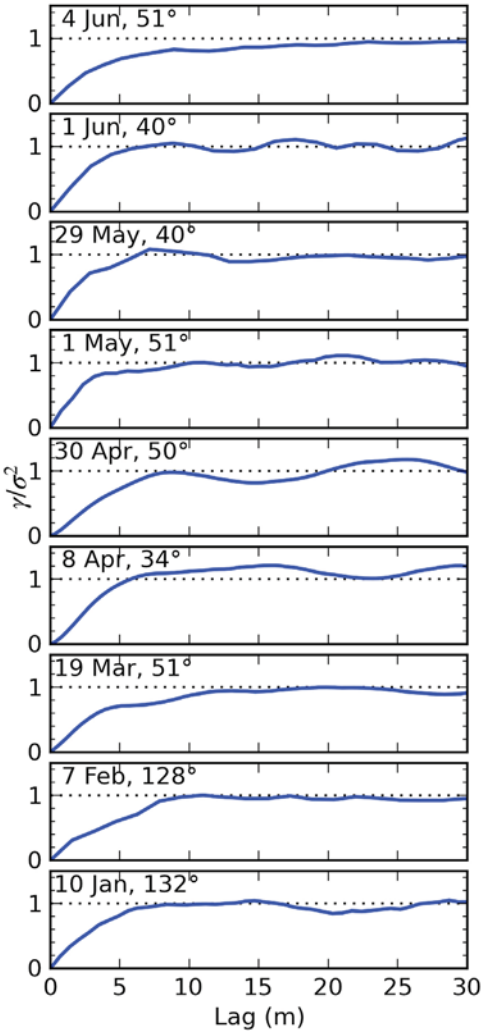

Figure 5. Variograms of transects in Figure 4, γ is scaled with the variance of the respective transect, σ^2. Dotted lines are drawn at $\gamma/\sigma^2 = 1.0$. Indicated are respective dates and direction.

standard deviation were 0.19 ± 0.06 m. Lidar data superimposed on the aerial photograph of 7 June show that the depth contours at 0.2 m align approximately with the outlines out melt ponds (Figure 9). In this figure, lidar data have been translated 0.85 m to the SSW.

[23] The progress of the early melt season is illustrated in Figure 10 along the albedo line, showing a relationship between initial meltwater pools and pond locations after initial drainage. Melt ponds were first recorded on 6 June and increased in areal extent until 11 June. Extent remained steady until drainage occurred from 14 to 15 June, reducing the areal extent. However, melt pond coverage increased again on 17 June.

[24] We performed a significance test of the collocation of dune locations and unponded islands by calculating the probability of the null hypothesis, i.e., a collocation as observed or higher resulting from a random choice of locations. The probability of the null-hypothesis is $p = 0.0003$, $p = 10^{-32}$, and $p = 10^{-23}$ for February, March and April, respectively. Accounting for the correlation length of the snow cover, we created 10000 randomly sub-sampled sets of dune locations, ensuring that no two locations within each set were within 10 m of each other. For 10000 randomly generated subsets, the probability that observations were due to chance was $p < 0.0008$ (45 dunes per subset), $p \leq 10^{-18}$ (73 to 88 dunes per subset) and $p \leq 10^{-10}$ (80 to 92 dunes per subset) in February, March and April, respectively.

[25] Since the spatial correlation function of islands in June was anisotropic, we repeated random subsampling using the shape of an ellipse around randomly selected dunes to exclude neighbors. From the shape of the correlation function shown in Figure 8a, we chose 50 m and 8 m as major and minor axis, respectively, with the major axis pointing along 76° east of North. In 99% of 10000 randomly generated subsets, the probability that observations were due to chance was $p < 0.2$ (25 to 28 dunes per subset), $p < 10^{-7}$ (33 to 44 dunes per subset) and $p < 0.0004$ (30 to 43 dunes per subset) in February, March, and April, respectively. The highest p-values found were 0.4, 2×10^{-7}, and 0.006 in February, March, and April, respectively.

[26] We will argue below that the high statistical significance (small p) in March and April, regardless of the subsampling strategy applied, is because snow dunes were precursors of ice islands.

4. Discussion

4.1. Snow Cover

[27] The evolution of the snow and ice surface was observed from four weeks after ice formation until two weeks into the melt pond formation period. The ice surface was undeformed and easterly winds prevailed. Between ice formation on 15 December and the first site visit on 9 January a thin snow cover of 0.05 m formed on the ice. While the snow cover was almost homogeneous on 9 January, snowfall and winds in excess of 10 m/s in the second half of January resulted in the formation of distinct snow dunes with a surface crust, some of them of barchanoid shape. In addition to the formation of the dunes, the mean snow depth had

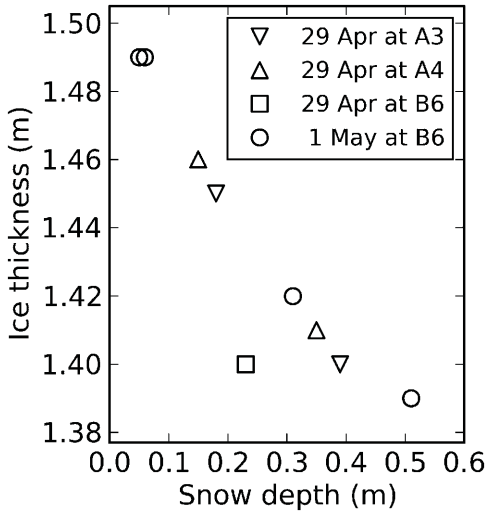

Figure 6. Observed ice thickness related to depth of snow depth. Locations A3, A4, and B6 are shown in Figure 1.

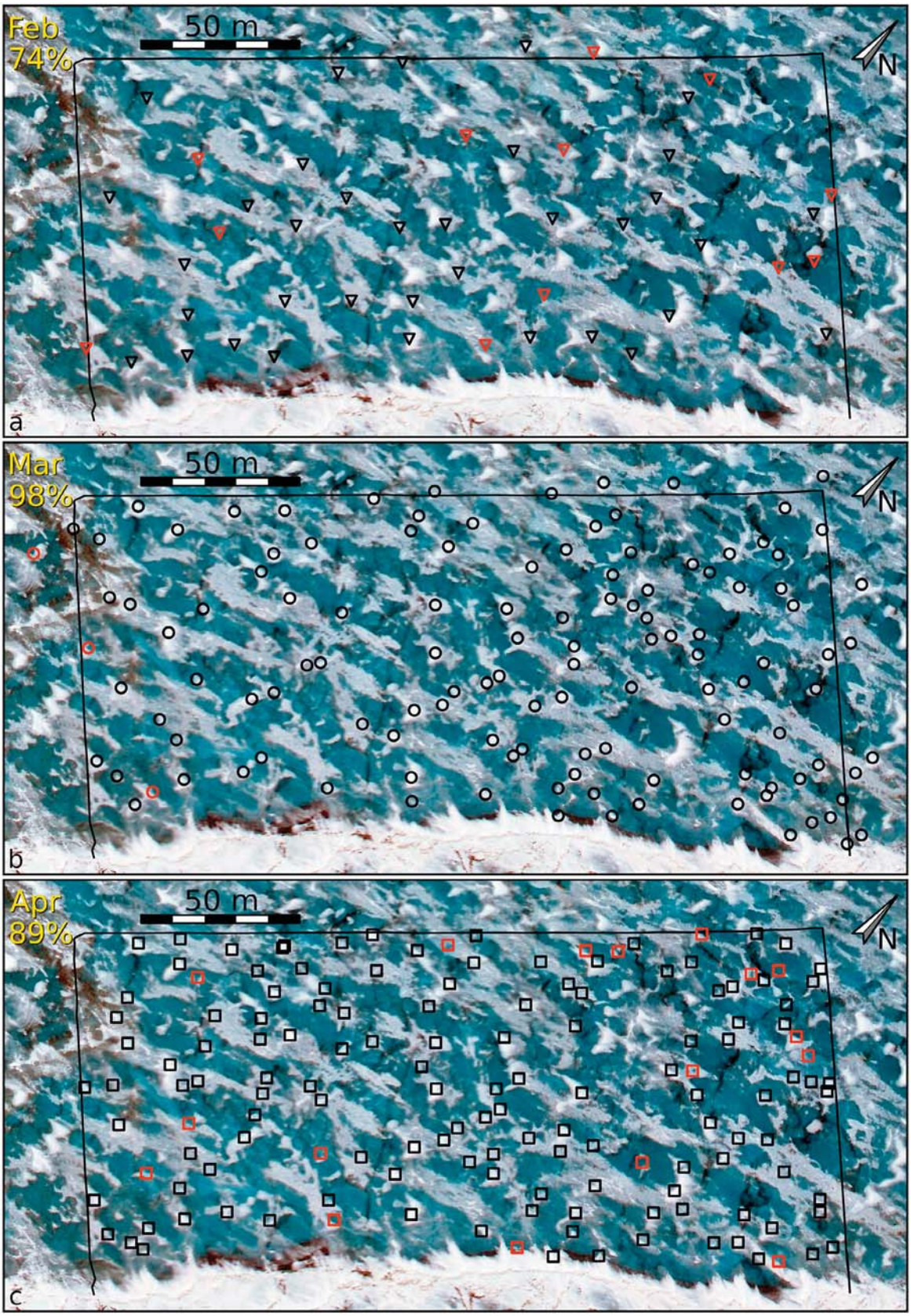

Figure 7. Superposition of aerial photographs of 7 June 2008 and dune locations of (a) 8 February (triangles), (b) 19 March (circles), and (c) 16 April (squares). Markers in black and red indicate dunes that do and do not correlate with islands, respectively. Percentage of correlated islands is indicated.

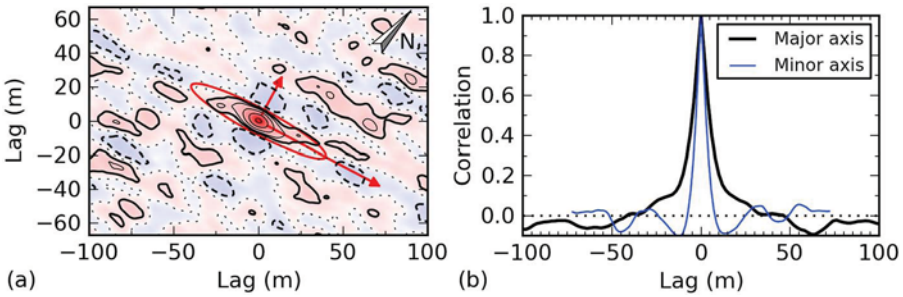

Figure 8. (a) Contour lines of the correlation function of the areal composite of 7 June (Figure 7). Contour lines are at −0.05 (dashed), 0 (dotted), 0.05 (thick solid), and 0.1, 0.2, 0.4, and 0.8 (thin solid lines). Red and blue shaded areas indicate regions of positive and negative autocorrelation, respectively. The red ellipse has major and minor axis of 50 m and 8 m, respectively, with major axis along 76° east of North, i.e., along the prevailing wind direction (Figure 2). Arrows indicate directions of major and minor axes. (b) Profile of correlation along major and minor axes.

increased significantly by this time. Based on our statistical analysis, the relationship of dune locations on 7 February to the melt ponds that developed in early June is less certain than for March and April. Precipitation later in February in conjunction with episodes of strong winds (frequently above 7 m/s) throughout February and March resulted in a further increase in dune height. The snow was wind-packed on 19 March and the lower inter-dune areas clearly correlated with the location of the melt ponds that formed 11 weeks later on 7 June. Precipitation, winds, and temperatures close to 0°C throughout April further affected the snow surface. Snow depth increased another 70% by 8 April and by another 5% by early May. The dunes recorded on 16 April showed a statistical correlation with early melt patterns similar to the March observations presumably because they were the same dunes and had not moved or migrated. The formation of the snow cover during distinct weather events is consistent with observations of *Sturm et al.* [2002] in the Arctic Ocean who observed that the formation of the most dominant slabs of snow took place during simultaneous wind and precipitation events. We noted at the end of April that the ice thickness under deep snow was less than under thin snow. Since this can be understood from the low thermal conductivity of snow compared to sea ice [*Maykut and Untersteiner*, 1971], it also supports the inference that the dunes were largely stationary during the ice growth season. Similar observations have been reported for landfast ice in the Beaufort Sea [*Barnes et al.*, 1979]. Stationarity was also found during the transition from snow dunes to a ponded surface. Lidar measurements of the two-dimensional snow depth profile on 7 May closely resembled the outline of meltwater patterns early in the melt season (7 June). While the lidar field was too small for a statistical analysis, dune locations recorded in March and April coincided with the locations of deeper snow recorded by the lidar. Snow ablation started in May, and meltwater pools first appeared on the surface on 6 June. Meltwater pools increased in aerial extent until 11 June (at which time the snow cover had completely melted off in the study plot, with the exception of snow along deformed ice at the margin), decreased and then increased again on 17 June, at the end of the campaign. While the development of melt pond aerial coverage is usually characterized by non-trivial increases and decreases throughout the melt season [e.g., *Perovich et al.*, 2007], the record at the albedo line indicates that early season meltwater patterns were related to the pond cover later in the season, at a time when surface ablation had removed the bulk of the snow cover and exposed underlying ice [see also *Polashenski et al.*, 2012].

4.2. Sensitivity

4.2.1. Location Measurement

[28] The sensitivity of the co-location of dunes and ice islands was tested to random perturbations of the coordinates of the dunes. WAAS-assisted GPS measurements are expected to be accurate at the meter-scale. Therefore, each recorded dune location was shifted randomly by up to 1.5 m from its original position (the areal probability density was homogeneous within a circle of radius 1.5 m). Based on 1000 realizations of randomly perturbed dune locations, mean and standard deviation of the co-locations with ice islands in June were (71 ± 5)%, (92 ± 2)%, and (84 ± 2)% in February, March, and April, respectively, i.e., approximately 5%-points lower than determined for the original

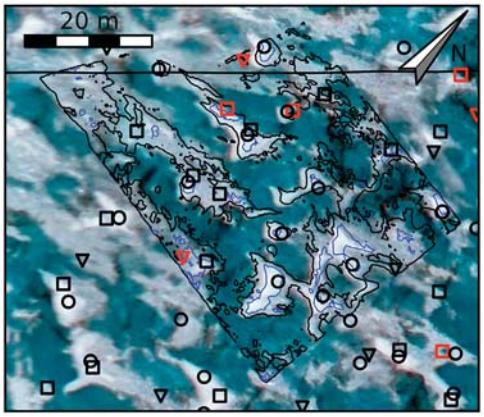

Figure 9. Comparison of lidar snow depth contour lines of 0.2 m (black) and 0.3 m (blue) with aerial photograph and locations of registered dunes of 8 February (triangles), 19 March (circles), and 16 April (squares). The horizontal line shows the position of the North-West edge of the dune field. Black and red markers indicate dune locations correlating and not correlating with islands, respectively.

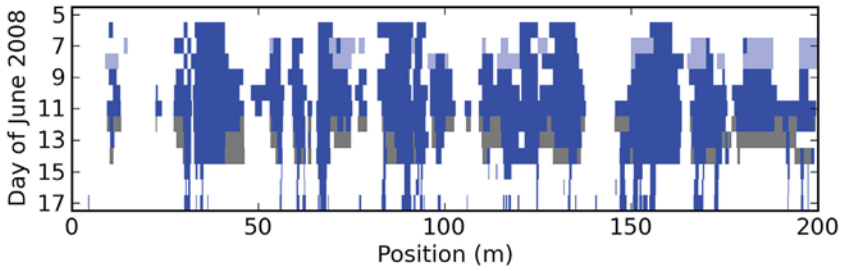

Figure 10. Development of surface characteristics along the albedo line (East to West) between 5 and 17 June 2008: snow, bare ice or white, decaying ice (white); slushy ice (light blue); melt pond (dark blue); suspended ice (gray).

dune locations. The standard deviation for February is highest because the number of dunes was lowest. Co-location is statistically significant at $p \leq 0.01$ even in February, assuming a co-location of one standard deviation below the mean (i.e., 66% in February). Hence, random errors in co-location of up to 1.5 m (in addition to presumably already present errors) would not have been sufficient to compromise the significance of the correlation between dunes and ice islands.

4.2.2. Threshold

[29] We chose an intensity threshold to identify islands based on the location of the minimum between the two modes of the histogram for the red channel. The choice of threshold value turns out not to be critical. Correlations in March and April are statistically significant at $p < 10^{-8}$ even for thresholds 16% above or below the selected intensity threshold (i.e., moving the position of the threshold halfway toward the peak of either mode), based on a 10 m-exclusion radius and 10000 randomly chosen subsets. For February, statistical significance is also high at $p < 0.0004$ and $p \leq 0.005$ for reduced and increased threshold values, respectively. Hence, the statistical analysis is insensitive to the method of discriminating ice islands from ponded surface.

4.2.3. Early Snow Distribution

[30] While the observed co-location between dunes and ice islands was significant in February ($p = 0.0003$), one robustness assessments discussed so far was far less compelling than for March or April: excluding measurements based on the autocorrelation function of the aerial image. Considering the island coverage of $q = 0.49$ on 7 June, the number of recorded dunes in February was small. This resulted in statistical significance strongly dependent on individual observations. For example, using the entire data set of measurements, the significance would have been less than compelling ($p \geq 0.01$) in February if 4 of the dunes had been co-located with water rather than ice islands. This is a comparatively small number, given that 46 and 44 dunes would have needed to be reclassified in March and April, respectively. This calls into question the robustness of statistical assessments for February. Apart from relying on a comparatively small absolute number of observations, the percentage of matches is also smallest for February observations. This could be due in part to the shape of the dunes. Islands in June were elongated parallel to the dominant wind direction. This alignment is also characteristic for a mature snowpack consisting of sastrugi. However, sastrugi were absent in February and some dunes in February were of barchanoid character, i.e., they were elongated perpendicular to the wind direction. Sastrugi tend to be shaped by winds from generally consistent but slightly variable directions, in this case by the particular winds of February and March. Their particular directions may have moved the point locations recorded for the dunes toward the periphery of the sastrugi.

5. Conclusion

[31] The evolution of the snow and ice surface of level sea ice was tracked from an initially almost featureless cover in January until the formation of melt ponds and removal of snow cover in June. The co-location between dunes in March and April and ice islands in June is certain. However, co-location of dunes in February and islands in June is very likely but not certain, calling for closer investigations of the early stages of snow cover evolution. The location of melt ponds was related to the snow cover 80 days (potentially 120 days) prior to the onset of melt pond formation. Ground-based lidar measurements in May showed that melt ponds began to form in the interstices between the dunes. The snow cover started to develop comparatively late in 2008, making it likely that correlations between snow and melt ponds exceed the period observed in this study in some years.

[32] The snow and melt pond conditions observed at Barrow appear to be representative for level landfast ice at a wide range of locations throughout the Arctic. The general shape and size of the stationary dunes studied at Barrow on stationary landfast ice appear to be similar to observations on landfast ice at Prudhoe Bay [e.g., *Barnes et al.*, 1979]. In addition, aerial surveys of the ponded surface showed elongated patterns similar to those on level landfast ice at Resolute Bay, and at Barrow in subsequent years [*Yackel et al.*, 2000; *Polashenski et al.*, 2012]. Observations may be transferable to moving pack ice. Like dunes on landfast ice, dunes on pack ice would be exposed to winds resulting in wind-packing and erosion [*Sturm et al.*, 2002], albeit due to winds from potentially more variable directions. Past work on drifting, level first-year ice is scarce [*Sturm et al.*, 2002]. Since long-term observations are challenging, in particular on comparatively thin first-year ice, stationary dunes could be identified through spatial correlation between snow depth and ice thickness.

[33] We demonstrated quantitatively that snow dunes influence melt pond evolution months before the onset of melt. Their location determines the meltwater distribution in the early stages of melt pond development on level first-year sea ice. Due to the lower albedo of meltwater-covered ice,

this ice shows higher rates of surface ablation than bare white ice, establishing a surface topography that forms the initial conditions for the later stages of melt pond evolution as shown in other studies [*Eicken et al.*, 2004; *Polashenski et al.*, 2012]. The early stages of melt pond formation on level first-year sea ice are therefore driven by snow depth distribution rather than sea ice surface topography.

[34] Given the importance of melt ponds in controlling ice albedo and hence the energy budget of ice-covered regions, this finding raises important questions on the impact of changes in spatial snow-depth variations, e.g., as a result of winter warming events or changed ice roughness, on summer ice albedo evolution and light transmission [cf. *Arrigo et al.*, 2012; *Perovich and Polashenski*, 2012; *Polashenski et al.*, 2012]. This calls for a systematic investigation of the development and both local and trans-Arctic variability of the snow cover. Further, in general circulation models, snow cover evolution should be considered as the driving mechanism for melt pond and albedo evolution in the early stages of melt on first-year sea ice.

[35] Moreover, since ponds tend to reoccur at the same locations as ice undergoes subsequent summer ablation cycles [*Eicken et al.*, 2001], the snow deposition regime on first-year sea ice that survives the summer may impact the ice radiation budget over the course of several years, lending urgency to better understanding of snow deposition and redistribution on sea ice.

[36] **Acknowledgments.** Data acquisition for this project was supported by the National Science Foundation Office of Polar Programs (awards OPP-0632398 and OPP-0856867). Chris Petrich would like to acknowledge an International Polar Year postdoctoral fellowship of the University of Alaska Foundation and the Research Council of Norway (project number 195153) that allowed for analysis of the data. Weather data were provided by the National Oceanic and Atmospheric Administration (NOAA). We wish to acknowledge staff at the Barrow Arctic Science Consortium (BASC) for excellent support of this project. Magnaprobe snow depth measurements on 1 May 2008 and some thickness measurements for Figure 6 were performed by volunteers of Ben and Jerry's Climate Change College. We are indebted to Martin Stuefer for providing us with the opportunity to take aerial photographs from his plane. The constructive comments of Ian Eisenman and two anonymous reviewers of an earlier version of this manuscript, and two anonymous reviewers of this manuscript are gratefully acknowledged.

References

Arrigo, K. R., et al. (2012), Massive phytoplankton blooms under Arctic sea ice, *Science*, *336*(6087), 1408, doi:10.1126/science.1215065.

Barnes, P. W., E. Reimnitz, L. Toimil, and H. Hill (1979), Fast ice thickness and snow depth relationships related to oil entrapment potential, Prudhoe Bay Alaska, paper presented at 5th International Conference on Port and Ocean Engineering Under Arctic Conditions, Norw. Inst. of Technol., Trondheim, Norway, 13–18 Aug.

Doumani, G. A. (1967), Surface structures in snow, in *Physics of Snow and Ice: Proceedings, International Conference on Low Temperature Science*, vol. 1, edited by H. Oura, pp. 1119–1136, Inst. of Low Temp. Sci., Sapporo, Japan.

Druckenmiller, M. L., H. Eicken, M. A. Johnson, D. J. Pringle, and C. C. Williams (2009), Toward an integrated coastal sea-ice observatory: System components and a case study at Barrow, Alaska, *Cold Reg. Sci. Technol.*, *56*(2–3), 61–72, doi:10.1016/j.coldregions.2008.12.003.

Eicken, H., W. B. Tucker III, and D. K. Perovich (2001), Indirect measurements of the mass balance of summer Arctic sea ice with an electromagnetic induction technique, *Ann. Glaciol.*, *33*, 194–200, doi:10.3189/172756401781818356.

Eicken, H., H. R. Krouse, D. Kadko, and D. K. Perovich (2002), Tracer studies of pathways and rates of meltwater transport through Arctic summer sea ice, *J. Geophys. Res.*, *107*(C10), 8046, doi:10.1029/2000JC000583.

Eicken, H., T. C. Grenfell, D. K. Perovich, J. A. Richter-Menge, and K. Frey (2004), Hydraulic controls of summer Arctic pack ice albedo, *J. Geophys. Res.*, *109*, C08007, doi:10.1029/2003JC001989.

Federal Aviation Administration (2008a), Wide area augmentation system performance analysis report, 1 January–31 March 2008, *Rep. 24*, 149 pp., Washington, D. C.

Federal Aviation Administration (2008b), Wide area augmentation system performance analysis report, 1 April–30 June 2008, *Rep. 25*, 150 pp., Washington, D. C.

Fetterer, F., and N. Untersteiner (1998), Observations of melt ponds on Arctic sea ice, *J. Geophys. Res.*, *103*(C11), 24,821–24,835, doi:10.1029/98JC02034.

Grenfell, T. C., and D. K. Perovich (2004), Seasonal and spatial evolution of albedo in a snow-ice-land-ocean environment, *J. Geophys. Res.*, *109*, C01001, doi:10.1029/2003JC001866.

Hanesiak, J. M., D. G. Barber, R. M. Abreu, and J. J. Yackel (2001), Local and regional observations of Arctic first-year sea ice during melt ponding, *J. Geophys. Res.*, *106*(C1), 1005–1016, doi:10.1029/1999JC000068.

Herzfeld, U. C., J. A. Maslanik, and M. Sturm (2006), Geostatistical characterization of snow-depth structures on sea ice near Point Barrow, Alaska—A contribution to the AMSR-Ice03 field validation campaign, *IEEE Trans. Geosci. Remote Sens.*, *44*(11), 3038–3056, doi:10.1109/TGRS.2006.883349.

Holt, B., and S. A. Digby (1985), Processes and imagery of first-year fast sea ice during the melt season, *J. Geophys. Res.*, *90*(C3), 5045–5062, doi:10.1029/JC090iC03p05045.

Iacozza, J., and D. G. Barber (2010), An examination of snow redistribution over smooth land-fast sea ice, *Hydrol. Processes*, *24*(7), 850–865, doi:10.1002/hyp.7526.

Light, B., T. C. Grenfell, and D. K. Perovich (2008), Transmission and absorption of solar radiation by Arctic sea ice during the melt season, *J. Geophys. Res.*, *113*, C03023, doi:10.1029/2006JC003977.

Lüthje, M., D. L. Feltham, P. D. Taylor, and M. G. Worster (2006), Modeling the summertime evolution of sea-ice melt ponds, *J. Geophys. Res.*, *111*, C02001, doi:10.1029/2004JC002818.

Massom, R. A., et al. (2001), Snow on Antarctic sea ice, *Rev. Geophys.*, *39*(3), 413–445, doi:10.1029/2000RG000085.

Maykut, G. A., and N. Untersteiner (1971), Some results from a time-dependent thermodynamic model of sea ice, *J. Geophys. Res.*, *76*(6), 1550–1575, doi:10.1029/JC076i006p01550.

Morassutti, M. P., and E. F. LeDrew (1996), Albedo and depth of melt ponds on sea-ice, *Int. J. Climatol.*, *16*, 817–838, doi:10.1002/(SICI)1097-0088(199607)16:7<817::AID-JOC44>3.0.CO;2-5.

Perovich, D. K. (1998), Optical properties of sea ice, in *Physics of Ice-Covered Seas*, vol. 1, edited by M. Leppäranta, pp. 195–230, Univ. of Helsinki, Helsinki.

Perovich, D. K., and C. Polashenski (2012), Albedo evolution of seasonal Arctic sea ice, *Geophys. Res. Lett.*, *39*, L08501, doi:10.1029/2012GL051432.

Perovich, D. K., S. V. Nghiem, T. Markus, and A. Schweiger (2007), Seasonal evolution and interannual variability of the local solar energy absorbed by the Arctic sea ice–ocean system, *J. Geophys. Res.*, *112*, C03005, doi:10.1029/2006JC003558.

Petrich, C., H. Eicken, J. Zhang, J. R. Krieger, Y. Fukamachi, and K. I. Ohshima (2012), Coastal landfast sea ice decay and break-up in northern Alaska: Key processes and seasonal prediction, *J. Geophys. Res.*, *117*, C02003, doi:10.1029/2011JC007339.

Polashenski, C. M., D. K. Perovich, and Z. Courville (2012), The mechanisms of sea ice melt pond formation and evolution, *J. Geophys. Res.*, *117*, C01001, doi:10.1029/2011JC007231.

Pomeroy, J. W. (1989), A process-based model of snow drifting, *Ann. Glaciol.*, *13*, 237–240.

Pomeroy, J. W., and D. M. Gray (1995), Snowcover accumulation, relocation and management, *Sci. Rep. 7*, 350 pp., Natl. Hydr. Res. Inst., Saskatoon, Sask., Canada.

Snyder, J. P. (1987), Map projections—A working manual, *U.S. Geol. Surv. Prof. Pap.*, *1395*, 385 pp.

Sturm, M. (2009), Field techniques for snow observations on sea ice, in *Field Techniques for Sea Ice Research*, edited by H. Eicken et al., pp. 25–47, Univ. of Alaska Press, Fairbanks.

Sturm, M., and J. A. Holmgren (1999) Self-recording snow depth probe, Patent 5864059, U.S. Patent and Trademark Off., Washington, D. C.

Sturm, M., J. Holmgren, and D. Perovich (2002), The winter snow cover on the sea ice of the Arctic Ocean at SHEBA: Temporal evolution and spatial variability, *J. Geophys. Res.*, *107*(C10), 8047, doi:10.1029/2000JC000400.

Watanabe, O. (1978), Distribution of surface features on snow cover in Mizuho Plateau, *Mem. Natl. Inst. Polar Res.*, *7*, 44–62.

Yackel, J. J., D. G. Barber, and J. M. Hanesiak (2000), Melt ponds on sea ice in the Canadian Archipelago: 1. Variability in morphological and radiative properties, *J. Geophys. Res.*, *105*(C9), 22,049–22,060, doi:10.1029/2000JC900075.